Fluence Correction Factors and Stopping Power Ratios for Clinical Ion Beams

Armin Lühr[1,2], David C. Hansen[2], Nikolai Sobolevsky[3], Hugo Palmans[4], Séverine Rossomme[5], and Niels Bassler[1,2]

[1] Department of Experimental Clinical Oncology, Aarhus University Hospital, Aarhus, Denmark

[2] Department of Physics and Astronomy, University of Aarhus, Aarhus, Denmark

[3] Department of Neutron Research, Institute for Nuclear Research of the Russian Academy of Sciences, Moscow 117312, Russia

[4] Division of Acoustics and Ionising Radiation, National Physical Laboratory, Teddington TW11 0LW, UK

[5] Centre for Molecular Imaging and Experimental Radiotherapy, Université Catholique de Louvain, Brussels, Belgium

E-mail: luehr@phys.au.dk; bassler@phys.au.dk

Abstract.

Background: In radiation therapy, the principal dosimetric quantity of interest is the absorbed dose to water. Therefore, a dose conversion to dose to water is required for dose deposited by ion beams in other media. This is in particular necessary for dose measurements in plastic phantoms for increased positioning accuracy, graphite calorimetry being developed as a primary standard for dose to water dosimetry, but also for the comparison of dose distributions from Monte Carlo simulations with those of pencil beam algorithms.

Material and Methods: In the conversion of absorbed dose to phantom material to absorbed dose to water the water-to-material stopping power ratios (STPR) and the fluence correction factors (FCF) for the full charged particle spectra are needed. We determined STPR as well as FCF for water to graphite, bone (compact), and PMMA as a function of water equivalent depth, z_{w}, with the Monte Carlo code SHIELD-HIT10A. Simulations considering all secondary ions were performed for primary protons as well as carbon, nitrogen and oxygen ions with a total range of 3, 14.5, and 27 cm as well as for two spread-out Bragg-peaks (SOBP). STPR as a function of depth are also compared to a recently proposed analytical formula.

Results: The STPR are of the order of 1.022, 1.070, and 1.112 for PMMA, bone, and graphite, respectively. STPR vary only little with depth except close to the total range of the ion and they can be accurately approximated with an analytical formula. The amplitude of the FCF depends on the non-elastic nuclear interactions and it is unity if these interactions are turned off in the simulation. Fluence corrections are of the order of a percent becoming more pronounced for larger depths resulting in dose difference of the order of 5% around 25 cm. The same order of magnitude is observed for SOBP.

Conclusions: We conclude that for ions with small total range ($z_{\mathrm{w-eq}} \leq 3\,\mathrm{cm}$) dosimetry without applying FCF could in principle be performed in phantoms of materials other than water without a significant loss of accuracy. However, in clinical high-energy ion beams with penetration depths $z_{\mathrm{w-eq}} > 15\,\mathrm{cm}$, where accurate positioning in water is not an issue, absorbed dose measurements should be directly performed in water or accurate values of FCF need to be established.

1. Introduction

Various applications require the conversion of dose to medium to dose to water in proton and carbon ion therapy. Since the quantity of interest for dose specification in radiotherapy is water, the quantity measured using non-water calorimeters (dose to the calorimeter medium) needs to be converted into dose to water. The potential for absolute dosimetry using graphite calorimeters has been demonstrated for protons [1] and carbon ions [2] and the National Physical Laboratory (NPL) is at present developing a primary standard level graphite calorimeter for proton and carbon ion beams. Also with the use of ionization chambers for reference dosimetry, such a dose conversion may be necessary for example when measurements have to be performed in plastic phantoms for reducing the positioning uncertainty. A need for dose conversion may also occur when dose plans obtained with Monte Carlo simulations [3], usually in terms of dose to tissue, should be directly compared to the dose distributions by pencil beam dose calculation algorithms, which usually calculate dose to water [4].

The conversion of dose to a medium to dose to water is predominantly governed by the medium over water stopping power ratio (STPR) which needs to be accurately known. In addition, if charged particle fluence distributions at equivalent depths in the medium and in water are not equal, a correction for this difference in fluence needs to be applied. For graphite calorimetry in low-energy protons, fluence correction factors (FCF) have been evaluated by experiment and Monte Carlo simulations [5] with the conclusion that FCF for a 60 MeV proton beam can be taken as unity with an uncertainty of 0.3%. For ionization chamber measurements in clinical proton beams, FCF for PMMA were obtained by experiment and Monte Carlo simulations [6]. A result of this study was the observation that fluence corrections are negligible for low-energy beams but can amount to several percent for high-energy proton beams. The water equivalence of various tissues for clinical cases has been investigated considering, e.g., the influence on the ion ranges [4, 7]. The results indicate

that fluence corrections of several percents could be required also for the application of comparing dose distributions obtained from Monte Carlo calculations and pencil beam algorithms. It was concluded in [4] that for proton beams stopping in bony anatomy, the predicted beam range can differ by 2-3 mm when comparing dose to tissue and dose to water.

For ions heavier than protons, the uncertainties of STPR are deemed to be larger than for protons and they were studied in a clinical context only for the specific case of water-to-air [8]. On the other hand, the influence of differences in fluence between media and water on the dose conversion, that is FCF, has not at all been investigated before.

In this paper, STPR and FCF with reference to water are calculated for graphite, PMMA and bone in proton, carbon ion, nitrogen ion, and oxygen ion beams using the Monte Carlo code SHIELD-HIT.

2. Materials and Methods

The quantity of interest in medical application is usually dose to water in water at a certain depth, z_{w}, that is $D_{\mathrm{w}}(z_{\mathrm{w}})$. The water-equivalent depth, $z_{\mathrm{w-eq}}$, for a particular depth in a different material, z_{m}, can be calculated using the ratio of the ion ranges in water and material, $r_{0,w}$ and $r_{0,m}$, respectively, as:

$$z_{\mathrm{w-eq}} = z_{\mathrm{m}} \frac{r_{0,\mathrm{w}}}{r_{0,\mathrm{m}}} \,. \tag{1}$$

The ranges of monoenergetic ions can be analytically approximated by the continuous slowing-down approximation (csda) while for spread-out Bragg-peaks (SOBP) the ranges were estimated as depths distal to the SOBP where the dose drops to 50% of the maximum.

2.1. Dose to material and dose to water

Monte Carlo simulations allow for the most direct determination of the conversion factor for dose in material to dose in water. The ratio of dose to water $D_{\mathrm{w}}(z_{\mathrm{w-eq}})$ in the water phantom and dose to material $D_{\mathrm{m}}(z_{\mathrm{m}})$ in a phantom of a material of interest can be derived from the

charged particle fluences $\Phi_{\mathrm{w},i}(E, z_{\mathrm{w-eq}})$ and $\Phi_{\mathrm{m},i}(E, z_{\mathrm{m}})$ differential in energy E, for all charged particle types i, in both phantom materials:

$$\frac{D_{\mathrm{w}}(z_{\mathrm{w-eq}})}{D_{\mathrm{m}}(z_{\mathrm{m}})} = \frac{\sum_i \int_0^{E_{\max,i}} \Phi_{\mathrm{w},i}(E, z_{\mathrm{w-eq}}) \left(\frac{S_i(E)}{\rho}\right)_{\mathrm{w}} \mathrm{d}E}{\sum_i \int_0^{E_{\max,i}} \Phi_{\mathrm{m},i}(E, z_{\mathrm{m}}) \left(\frac{S_i(E)}{\rho}\right)_{\mathrm{m}} \mathrm{d}E}\,, \tag{2}$$

where $\frac{S_i(E)}{\rho}$ are the electron collision stopping powers for particle type i and ρ is the density of the material. Equation (2) is exact when all charged particles are considered (i.e. also those produced by neutron interactions) and the fluence distributions are obtained by tracking all charged particles down to zero kinetic energy.

Alternatively, Monte Carlo simulations can provide corrections to the simplified assumption that the charged particle fluence distributions at equivalent depths in both phantom materials are equal, i.e. $\Phi_{E,\mathrm{w},i} = \Phi_{E,\mathrm{m},i}$ for all energies E and all charged particle types i. If this assumption is fulfilled, $D_{\mathrm{m}}(z_{\mathrm{m}})$ and $D_{\mathrm{w}}(z_{\mathrm{w-eq}})$ were simply related as

$$D_{\mathrm{w}}(z_{\mathrm{w-eq}}) = D_{\mathrm{m}}(z_{\mathrm{m}})\, S_{w/m}(\Phi_{\mathrm{m}}[z_{\mathrm{m}}]) \tag{3}$$

by the water-to-air mass electron collision STPR,

$$S_{\mathrm{w/m}}(\Phi_{\mathrm{m}}[z_{\mathrm{m}}]) = \frac{\sum_i \int_0^{E_{\max,i}} \Phi_{m,i}(E, z_{\mathrm{m}}) \left(\frac{S_i(E)}{\rho}\right)_{\mathrm{w}} \mathrm{d}E}{\sum_i \int_0^{E_{\max,i}} \Phi_{m,i}(E, z_{\mathrm{m}}) \left(\frac{S_i(E)}{\rho}\right)_{\mathrm{m}} \mathrm{d}E}\,, \tag{4}$$

for the total charged particle fluence distribution Φ_{m} in the material. Recently, an analytical expression for STPR was proposed [8],

$$\tilde{S}_{\mathrm{w/m}}(z) = \frac{\left\langle \frac{Z}{A} \right\rangle_{\mathrm{w}}}{\left\langle \frac{Z}{A} \right\rangle_{\mathrm{m}}} \frac{\ln[E_0/I_{\mathrm{w}}] + 1/k \ln\left[1 - z/r_0\right] + 7.6863}{\ln[E_0/I_{\mathrm{m}}] + 1/k \ln\left[1 - z/r_0\right] + 7.6863}\,, \tag{5}$$

for arbitrary material combinations and primary ions. Here, E_0 is the initial energy of the ions in MeV/u, I_{w} and I_{m} are the mean excitation energies in eV of water and a given medium, respectively. $\left\langle \frac{Z}{A} \right\rangle$ is the average ratio of the atomic number Z and relative atomic mass A of all atoms in the target medium weighted according to their fraction by weight and k is a dimensionless factor which is here set to $k = 1.7$ in accordance with [8].

However, in general the fluence distributions are not equal in both phantoms and a FCF needs to be introduced. Following a previous study [6], dose to water in water and dose to medium in the given medium at equivalent depths are related as:

$$D_{\mathrm{w}}(z_{\mathrm{w-eq}}) = D_{\mathrm{m}}(z_{\mathrm{m}})\, S_{w/m}(\Phi_{\mathrm{m}}[z_{\mathrm{m}}])\, k_{\mathrm{fl}}\left(\Phi_{\mathrm{w}}[z_{\mathrm{w-eq}}], \Phi_{\mathrm{m}}[z_{\mathrm{m}}]\right) \tag{6}$$

with the FCF,

$$k_{\mathrm{fl}}\left(\Phi_{\mathrm{w}}, \Phi_{\mathrm{m}}\right) = \frac{\sum_i \int_0^{E_{\mathrm{max},i}} \Phi_{\mathrm{w},i}(E, z_{\mathrm{w-eq}}) \left(\frac{S_i(E)}{\rho}\right)_{\mathrm{w}} \mathrm{d}E}{\sum_i \int_0^{E_{\mathrm{max},i}} \Phi_{\mathrm{m},i}(E, z_{\mathrm{m}}) \left(\frac{S_i(E)}{\rho}\right)_{\mathrm{w}} \mathrm{d}E} \tag{7}$$

as defined in [5]. The factor k_{fl} could be interpreted as the conversion of dose to water in the material phantom, to dose to water at an equivalent depth in the water phantom.

2.2. SHIELD-HIT

The presented results are obtained with Monte Carlo transport code simulations using SHILED-HIT [9, 10]. The most recent version SHIELD-HIT10A [11, 12] with an improved description of nuclear interactions [13] was used to simulate between 4×10^6 and 4×10^7 primary ions in order to obtain sufficient statistics. The initial energies were adjusted to obtain for all ions the same three total water equivalent ranges 30 mm, 145 mm, and 275 mm in cylindrical phantoms of 400 mm diameter and 300 mm length. Nuclear fragments resulting from non-elastic nuclear reactions were simulated down to 25 keV. Water stopping powers, calculated with a Bethe-Bloch formula as in the stopping power computer library *libdEdx* [14], were based on the errata to ICRU Report 73 [15] with a mean excitation energy $I = 78$ eV, while the stopping powers, material compositions, and densities for the other materials were based on the ICRU Report 49 [16] with the I-values 74 eV, 78 eV, and 91.9 eV for polymethyl methacralate (PMMA), graphite, and bone (compact, ICRU), respectively. The ion transport included Vavilov-Landau energy straggling and Molière multiple scattering. Note, SHIELD-HIT does not consider secondary electrons in detail and they are therefore not part of the full particle spectrum in this study.

The concept of virtual scoring, introduced in SHIELD-HIT10A, allows for a parallel detector geometry avoiding the dependence on artificial physical geometries and region boundaries. Furthermore, STPR and FCF are determined *on-line*, that is, during the transport of the particles reducing the influence on the result due to a spectral resolution limited by a finite number of energy intervals and post processing. A cylindrical detector geometry was used with a diameter of 200 mm and a water equivalent length of 300 mm divided into 0.1 mm thick slabs.

In this study, we also present calculations from two single field carbon ion SOBP being 3-dimensional dose cubes with equal side lengths. The way how SOBP are handled by SHIELD-HIT10A is described in [8, 12]. Here, the dose optimization was realized with the treatment planning software for particles TRiP [17] requesting one SOBP with flat physical and one with flat biological equivalent dose. The raster-scan file produced by TRiP describes the needed amount of particles for each raster point and for each energy slice. This file provides the necessary input for SHIELD-HIT to generate the radiation field for the SOBP at the surface of the phantom which is then transported in the SHIELD-HIT simulation through the phantom. A ripple filter implementation based on the design described in [18] is available in SHIELD-HIT10A [12] in order to smooth the SOBP.

3. Results

In Fig. 1 STPR for water to the materials graphite, PMMA, and bone for 270 MeV/u carbon ions are presented. The SHIELD-HIT10A simulations are compared to the analytical expression in Eq. (5) proposed in [8]. The same I-values which were used in the SHIELD-HIT10A simulation were also used for the analytical expression for STPR. For all three materials $S_{\mathrm{w/m}}(z_{\mathrm{w-eq}})$ can be reproduced by the analytical expression and practically no difference can be observed proximal to the Bragg-peak on the scale displayed in Fig. 1. For example, for PMMA the relative difference between simulation and formula varies from

0.01% at $z_{\mathrm{w-eq}} \approxeq 0$ down to 0.005% at $z_{\mathrm{w-eq}} = 14\,\mathrm{cm}$.

A depth-dose distribution of a SOBP for carbon ions in water calculated with SHIELD-HIT10A is shown in Fig. 2(a). The fluence of the primary ions at the surface of the phantom was taken from dose optimization for a flat physical dose performed with TRiP as described in Sec. 2.2. Also shown are the dose to water in medium curves $D_{\mathrm{w}}(z_{\mathrm{w-eq}})$ for the same initial fluence distribution at the surface of graphite, PMMA, and bone phantoms. The dose to water in medium distributions were obtained with Eq. (3), i.e. without FCF, using only the water-to-medium STPR at $z_{\mathrm{w-eq}}$ for this SOBP. These STPR are also shown in Fig. 2(b). Significant differences can be observed between the depth-dose distributions in the three materials and water which become more pronounced towards the distal end of the SOBP. Differences of 0 - 5% show up in the distal 20% of the SOBP region, i.e. 14 cm $\leq z_{\mathrm{w-eq}} <$ 15 cm, for both graphite and bone.

Figure 3(a) shows the physical depth-dose distribution of a SOBP for carbon ions simulated with SHIELD-HIT10A which was obtained with an initial fluence at the phantom surface optimized with TRiP to provide a flat biological dose equivalent using the local effect model [19]. The dose to medium in medium in the graphite, PMMA, and bone phantoms is again converted to dose to water in medium using only the water-to-medium STPR at $z_{\mathrm{w-eq}}$ for this SOBP shown in Fig. 3(b) The deviations of dose to water among the four materials water, graphite, PMMA, and bone vary with depth between 0 and 5%. However, no clear trend with depth or for a specific medium can be found for the biologically optimized SOBP. In contrast, all considered STPR show a clear and uniform behavior with depth. No pronounced differences can be observed between the STPR for the biologically and physically optimized SOBP in Figs. 3(b) and Fig. 2(b), respectively, on the displayed scale. Though, the peaks of the STPR occurring around the distal end of the SOBP appear to be narrower and more pronounced in the case of the physically optimized SOBP.

FCF in graphite for monoenergetic protons, carbon ions, nitrogen ions and oxygen ions

are presented in Figs. 4(a), (b), (c), and (d), respectively. The FCF were obtained according to Eq. (7) simulating full fluence distributions in water and in graphite. For small depth, $0 \lesssim z_{\mathrm{w-eq}}$ the FCF is always close to 1 and at the distal end of the Bragg-peak the FCF falls off steeply. The corrections due to the differences of the fluences vary with depth and are of the order of percent with about 5% at the maximal range for the highest energies considered here. While there are qualitative trends among curves for the same ion species, no general trend can be observed which is shared by all ions.

Figures 5(a) and 5(b) show FCF in PMMA for monoenergetic protons and carbon ions. For PMMA FCF are very close to 1 and even for larger depth $z_{\mathrm{w-eq}} \leq 25\,\mathrm{cm}$ the fluence corrections are below 1%. Within the first cm the corrections for protons are below 0.3% for initial energies below 150 MeV/u and can be completely neglected for carbon ions even at the highest energy of 400 MeV/u. Only in the vicinity of the Bragg-peak the fluence corrections become as large as 3% and 7% for protons and carbon ions, respectively.

FCF in bone for monoenergetic protons and carbon ions are presented in Figs. 6(a) and 6(b). The corrections for protons in bone are throughout small and below 1% except for in the vicinity of the Bragg-peak. In general, the results for carbon ions on bone resemble to a certain extent those for carbon ions on graphite in Fig. 4(b). For carbon ions the bone FCF curves decrease nearly linearly with depths, all having the same slope. Therefore, the fluence corrections are small close to the phantom surface but for large depths the FCF considerably deviate from unity, e.g. 5% at 25 cm. As a result, the corrections to dose to water are not much larger than 0.5% when a monoenergetic proton or carbon ion passes a bony structure with a thickness of up to 2 cm highlighted by the insets in Fig. 6.

Figure 7(a) shows the FCF for graphite for carbon ions obtained with Eq. (7) when non-elastic nuclear interactions are switched off in the SHIELD-HIT simulation. Under these conditions practically no effect can be observed up to about 95% of the total range for all energies. In order to estimate the influence of the primary ions on the total fluence

corrections compared to the influence of the secondary particles, Fig. 7(b) shows the fluence corrections in graphite exclusively for the primary carbon ions. The presented curves decrease linearly up to 75% of the total range. Compared to the correct FCF in Fig. 4(b), obtained as a sum over all particle types i, the partial fluence corrections only for the primary ions are more pronounced.

4. Discussion

The comparison of dose to water distributions in medium, obtained with Eq. (3), to dose to water in water for the SOBP in Figs. 2 and 3 shows that STPR alone are not sufficient to convert dose to medium in medium to dose to water in water. In addition, FCF are needed to convert dose to water in medium to dose to water in water. Comparing the physically and biologically optimized SOBP it can be observed that the relative deviations among the four dose to water curves are different for both SOBP. The deviations for both SOBP also vary differently with depth suggesting a non-trivial dependence of the FCF on the fluence spectra. Accordingly, a more systematic study especially of FCF for monoenergetic ion beams should be performed here in order to explain these differences.

4.1. Fluence correction factors

The results presented in Sec. 3 show that FCF primarily depend on the non-elastic nuclear cross sections which lead to a different fluence spectrum in the material than in water. If the non-elastic cross sections are turned off in the simulation the correction becomes basically zero as demonstrated in Fig. 7(a). The performed simulations show that FCF depend on the type and energy of the primary ions. But there is also a pronounced dependence of FCF on the detailed spectrum of all secondary particles. It is not possible to approximate or even reproduce the FCF for carbon ions on graphite in Fig. 4(b) with the corrections only for the fluence of the primary ions presented in Fig. 7(b). There is a subtle dependence on the full

particle spectrum in material compared to that in water which may also lead to cancellation of corrections originating from different particle types. This dependence on the spectra prevents from a simple analytical scaling of FCF with depth and energy for arbitrary primary ions and target materials which, in contrast, was possible to propose for STPR [8]. Consequently, more sophisticate techniques such as Monte Carlo simulations are required.

A linear trend with depth was earlier found for protons in [6] when using non-elastic cross sections from Janni [20]. However, when cross sections from ICRU 63 [21] were used the FCF were not linear with depth, similar to what is observed in the present study. Here, a number of FCF curves show a linear trend in an intermediate range starting at a depth of a couple of cm up to a depth of some cm before the Bragg-peak. In the vicinity of the Bragg-peak, however, it is difficult to obtain accurate correction values for a monoenergetic ion beam due to the high sensitivity of the results on the range scaling which was also discussed for proton beams in [5].

The fluence correction is in general very close to zero at the surface, as one can expect, since there the fluences in the material and water should hardly differ. However, it seems that it is still always smaller than zero where the deviations of FCF from unity are most pronounced for protons and are larger than 0.5% in the case of graphite. A deviation from unity was also observed for protons in Refs. [5–7]. There, it was explained to be caused by an incorrect conversion of contributions to the dose by secondary particles from nuclear interactions. Instead of scaling the total dose in material with the water-to-material STPR as in Eq. (7) it might be more appropriate to only scale the contribution due to electron and elastic nuclear interactions with STPR and the contribution from non-elastic nuclear interactions with the total nuclear cross sections per nucleon. However, this procedure might be impractical if one cannot distinguish the two different contributions to the dose and at the same time it seems to be less important for ions heavier than protons. This might be caused by the fact that the stopping power for ions with charge Z_p approximately scales with Z_p^2 and

253 therefore, the relative contribution from non-elastic interactions to the total dose to material
254 may decrease for ions with larger Z_p.

255 A significant decrease of FCF can be observed if the target material consists to a
256 substantial amount of the same nuclei as the primary ions. Examples can be found in Figs.
257 4(b), 7(b), and 6(b) for carbon ions on graphite (with and without contributions of secondary
258 particles) and carbon ions on bone, respectively, where the fraction by weight of carbon in
259 bone is about 27.8% [16]. This effect on FCF is inverted for oxygen ions on graphite in Fig.
260 4(d) because there the water target consists of about 88.8% of oxygen by weight [16]. This
261 effect can be observed most pronounced in the case that only the fluence of the primary
262 particles is considered, i.e. no interference from other particle types occurs. Then it is clear,
263 considering the definition of FCF for this case, that the fluence of the primary particles
264 decreases slower in the target which consists of the same nuclei as the primary ions. The
265 reduction of the non-elastic nuclear cross sections in this situation may be caused by
266 Pauli-blocking [22] or a resonance effect in the non-elastic nuclear cross sections. Following
267 this argument no pronounced increase or decrease would be expected for FCF for other ions
268 such as nitrogen on graphite since there is no fraction of nitrogen in water nor in graphite.
269 The fluence corrections for nitrogen ions on graphite shown in Fig. 4(c) are indeed small.
270 Therefore, they are consistent with the discussed suppression of nuclear fragmentation. The
271 observed effect is definitely of interest and a more detailed study would be helpful to fully
272 resolve its origin. Furthermore, it might be worth studying FCF for neutral primary particles
273 such as neutrons and their possible relevance for studies on neutron dosimetry such
274 as [23, 24].

275 *4.2. Stopping power ratios*

276 STPR are important for converting dose to material to dose to water in material due to their
277 order of magnitude which can lead to a difference between the two doses being larger than

10% such as for water-to-graphite STPR which can be much larger than due to FCF. On the other hand, the relative variation of STPR with depth is small compared to FCF. In the clinical context, STPR practically do not depend on the initial energy and primary ion, when they are considered as a function of residual range as was shown in Refs. [8, 14] for pristine and SOBP. Obviously, they are directly dependent on the electron collision stopping power and their accuracy is therefore dependent on the uncertainty of the used stopping-power data, which can be of the order of 1-2%, discussed in a recent detailed study for water-to-air STPR [8]. On the other hand, the considered STPR are nearly independent of the non-elastic nuclear cross sections, also observed earlier for other STPR [8, 25], which is exactly in opposition to what has been observed here for FCF. Thus, details of the full fluence spectrum obtained with SHIELD-HIT are of minor importance for STPR. The simple analytical expression given in Eq. (5), proposed in a study on water-to-air STPR [8], is sufficient to reproduce the Monte Carlo simulations as clearly demonstrated in Fig. 1 for carbon ions within 0.01%. As a result, STPR for arbitrary combinations of materials as well as primary ions can conveniently be obtained as a function of depth with the analytical expression in Eq. 5. This may also include other STPR relevant for standard dosimetry with air-filled or graphite detectors and phantom materials such as PMMA and polystyrene. Note, no detailed description of the contribution to STPR from secondary electrons generated along the particle tracks is possible with SHIELD-HIT. For the lightest primary ions, protons, with $Z_p = 1$ an increase of only up to 0.6% of the STPR due to secondary electrons was reported in [25]. For ions with higher charges the influence of the electrons on the STPR can be expected to become smaller since the stopping power scales approximately with the square of the particle charge. It would be helpful if this qualitative estimate is verified and quantified in a further study.

4.3. Dosimetry with non-water phantoms

So far, non-water phantoms, such as plastic or graphite phantoms, are not recommended by most dosimetry protocols, neither for reference nor for relative dosimetry. The reason for this are the required water to medium fluence correction factors which were not available for ions. Therefore, the results of the present work contribute in this matter making the use of non-water phantoms in principle possible for particle beams. Currently, it is intended to include proton and ion dosimetry with non-water phantoms in some future protocols.

For all studied ions and materials with a small total range ($z_{\mathrm{w-eq}} \leq 3\,\mathrm{cm}$) dosimetry without applying fluence corrections factors could in principle be performed in phantoms of materials other than water without a dramatic loss of accuracy. But in particular PMMA targets can be considered as a good candidate for dose to water measurements for ions at small depths, where accurate positioning in water may be a serious issue. For PMMA under these conditions, fluence correction factors and stopping power ratios are close to unity for all initial energies for protons as well as for heavier ions. On the other hand, in clinical high-energy ion beams with penetration depths $z_{\mathrm{w-eq}} > 15\,\mathrm{cm}$, where accurate positioning is not an issue, substantial correction factors would be needed and under these conditions it is advisable to perform measurements of absorbed dose directly in water. Otherwise accurate values of the fluence correction factors need to be established.

In summary, the Monte Carlo transport code SHIELD-HIT10A has been used to simulate fluence corrections factors and stopping power ratios necessary to convert absorbed dose to material in absorbed dose to water for a number of different combinations of ions and targets. Stopping power ratios depend primarily on electromagnetic interactions and therefore on the used stopping power data. They can be reproduced with an analytical formula with high precision. Fluence correction factors depend on the other hand on non-elastic nuclear interactions and become usually more pronounced with increasing depth. In general, we may conclude that dosimetry with non-water phantoms could be performed

under certain conditions. However, one has to be more cautious for heavier ions when relating dose to material to dose to water than it has earlier been advised for protons since the fluence corrections depend on the specific non-elastic nuclear cross sections of the ions and targets and the full particle spectrum has to be considered. Here, experimental data also for ions heavier than protons would clearly contribute to an improved understanding.

Acknowledgments

This work is supported by the Danish Cancer Society (http://www.cancer.dk), and the Lundbeck Foundation Centre for Interventional Research in Radiation Oncology (http://www.cirro.dk).

References

[1] Palmans H, Thomas R, Simon M, Duane S, Kacperek A, DuSautoy A, et al. A small-body portable graphite calorimeter for dosimetry in low-energy clinical proton beams. Phys Med Biol. 2004;49(16):3737.

[2] Sakama M, Kanai T, Fukumura A, Abe K. Evaluation of w values for carbon beams in air, using a graphite calorimeter. Phys Med Biol. 2009;54(5):1111–1130.

[3] Rosenschöld PMA, Aznar MC, Nygaard DE, Persson GF, Korreman SS, Engelholm SA, et al. A treatment planning study of the potential of geometrical tracking for intensity modulated proton therapy of lung cancer. Acta Oncol. 2010;49(7):1141–1148.

[4] Paganetti H. Dose to water versus dose to medium in proton beam therapy. Phys Med Biol. 2009;54(14):4399.

[5] Palmans H, Al-Sulaiti L, Andreo P, Thomas RAS, Shipley DR, Martinkovič J, et al. Conversion of dose-to-graphite to dose-to-water in a clinical proton beam. In: Proc. Int. Symp. on Standards, Applications and Quality Assurance in Medical Radiation Dosimetry IAEA-CN-182/277. Vienna, Austria: IAEA; submitted 2011. .

[6] Palmans H, Symons JE, Denis JM, de Kock EA, Jones DTL, Vynckier S. Fluence correction factors in plastic phantoms for clinical proton beams. Phys Med Biol. 2002;47(17):3055.

[7] Palmans H, Verhaegen F. Assigning nonelastic nuclear interaction cross sections to Hounsfield units for Monte Carlo treatment planning of proton beams. Phys Med Biol. 2005;50(5):991.

[8] Lühr A, Hansen DC, Jäkel O, Sobolevsky N, Bassler N. Analytical expressions for water-to-air stopping-power ratios relevant for accurate dosimetry in particle therapy. Phys Med Biol. 2011;56:2515–2533.

[9] Sobolevsky N. SHIELD-HIT Home page; 2011. [Online] latest status: http://www.inr.ru/shield/ [7 April 2011].

[10] Gudowska I, Sobolevsky N, Andreo P, Belkić D, Brahme A. Ion beam transport in tissue-like media using the Monte Carlo code SHIELD-HIT. Phys Med Biol. 2004;49:1933–1958.

[11] Hansen DC, Lühr A, Sobolevsky N, Bassler N. SHIELD-HIT 10A; 2010. [Online] latest status: http://aptg-trac.phys.au.dk/shieldhit [7 April 2011].

[12] Hansen DC, Lühr A, Herrmann R, Sobolevsky N, Bassler N. Recent Improvements in the SHIELD-HIT Code. Submitted to Int J Rad Biol. 2011;.

[13] Hansen DC, Lühr A, Sobolevsky N, Bassler N. Benchmarking nuclear models in SHIELD-HIT. in preparation. 2011;.

[14] Lühr A, Toftegaard J, Kantemiris I, Hansen DC, Bassler N. Stopping power: the generic library libdEdx and a study of clinically relevant stopping-power ratios for different ions. Int J Rad Biol. 2011;accepted for publication.

[15] Sigmund P, Schinner A, Paul H. Errata and Addenda: ICRU Report 73 (Stopping of ions heavier than helium). J ICRU. 2009;5. [Online] Available: http://www.icru.org/index.php?option=com_content&task=view&id=167.

[16] ICRU Report 49. Stopping powers and ranges for protons and alpha particles. Bethesda, MD: International Commission on Radiation Units and Measurements; 1993.

[17] Krämer M, Jäkel O, Haberer T, Kraft G, Schardt D, Weber U. Treatment planning for heavy-ion radiotherapy: physical beam model and dose optimization. Phys Med Biol. 2000;45:3299–3317.

[18] Weber U, Kraft G. Design and construction of a ripple filter for a smoothed depth dose distribution in conformal particle therapy. Phys Med Biol. 1999;44:2765–2775.

[19] Scholz M, Kraft G. Track Structure and the Calculation of Biological Effects of Heavy Charged Particles. Adv Space Res. 1995;18(1/2):(1/2)5–(1/2)14.

[20] Janni JF. Energy loss, range, path length, time-of-flight, straggling, multiple scattering, and nuclear interaction probability : In two parts. Part 1. For 63 compounds Part 2. For elements $1 \leq Z \leq 92$. Atom Data and Nucl Data Tables. 1982;27(2-3):147 – 339.

[21] ICRU Report 63. Nuclear Data for Neutron and Proton Radiotherapy and for Radiation Protection. Bethesda, MD: International Commision on Radiation Units and Measurements; 2000.

[22] Hartnack C, Puri RK, Aichelin J, Konopka J, Bass SA, Stöcker H, et al. Modelling the many-body dynamics of heavy ion collisions: Present status and future perspective. Eur Phys J A. 1998;1:151–169.

[23] Bassler N, Holzscheiter MH, Petersen JB. Neutron Fluence in Antiproton Radiotherapy, Measurements and Simulations. Acta Oncol. 2010;49:1149–1159.

[24] Schmitz T, Blaickner M, Schütz C, Wiehl N, Kratz JV, Bassler N, et al. Dose calculation in biological samples in a mixed neutron-gamma field at the TRIGA reactor of the University of Mainz. Acta Oncol. 2010;49(7):1165–1169.

[25] Medin J, Andreo P. Monte Carlo calculated stopping-power ratios, water/air, for clinical proton dosimetry (50 - 250 MeV). Phys Med Biol. 1997;42(1):89.

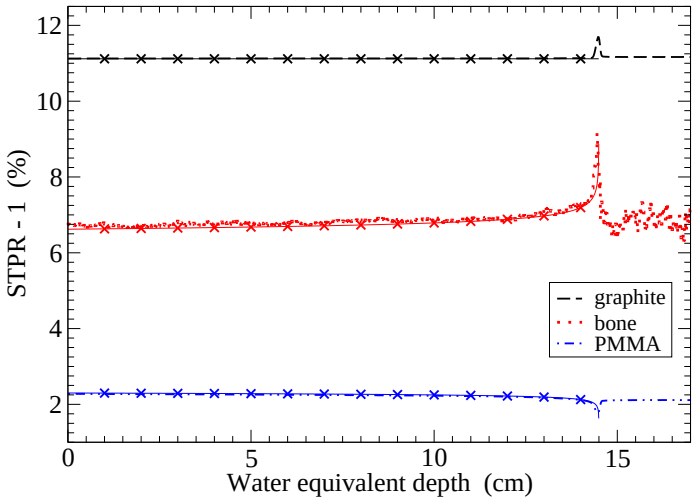

Figure 1. Water-to-material stopping power ratios for the materials graphite, PMMA, and bone for 270 MeV/u carbon ions. Results obtained with SHIELD-HIT10A are compared to stopping power ratios calculated with the analytical expression in Eq. (5). The analytical results are shown as a thin solid line with $\times$.

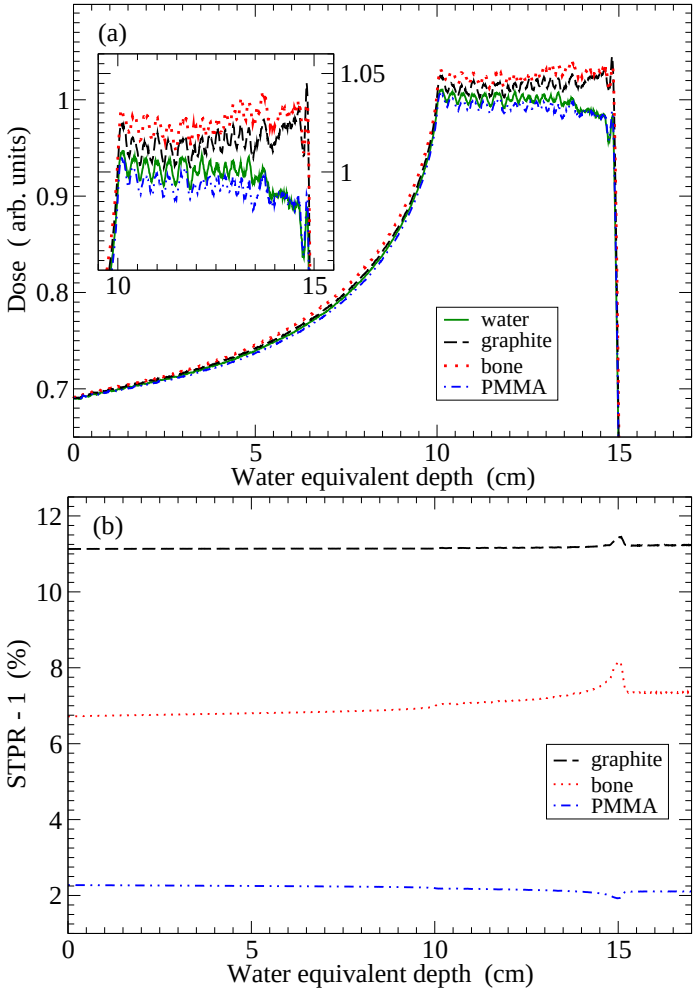

Figure 2. Detail of a carbon ion spread-out Bragg-peak optimized for a flat *physical dose* distribution in water with TRiP [17]. See the text for explanation. (a) SHIELD-HIT10A simulated depth-dose distributions in water, graphite, PMMA, and bone. The dose in the materials graphite, PMMA, and bone are converted to a dose to water with Eq. (3), i.e. without fluence correction factor. The inset shows the peak region enlarged. (b) Stopping power ratios for water to the materials graphite, PMMA, and bone.

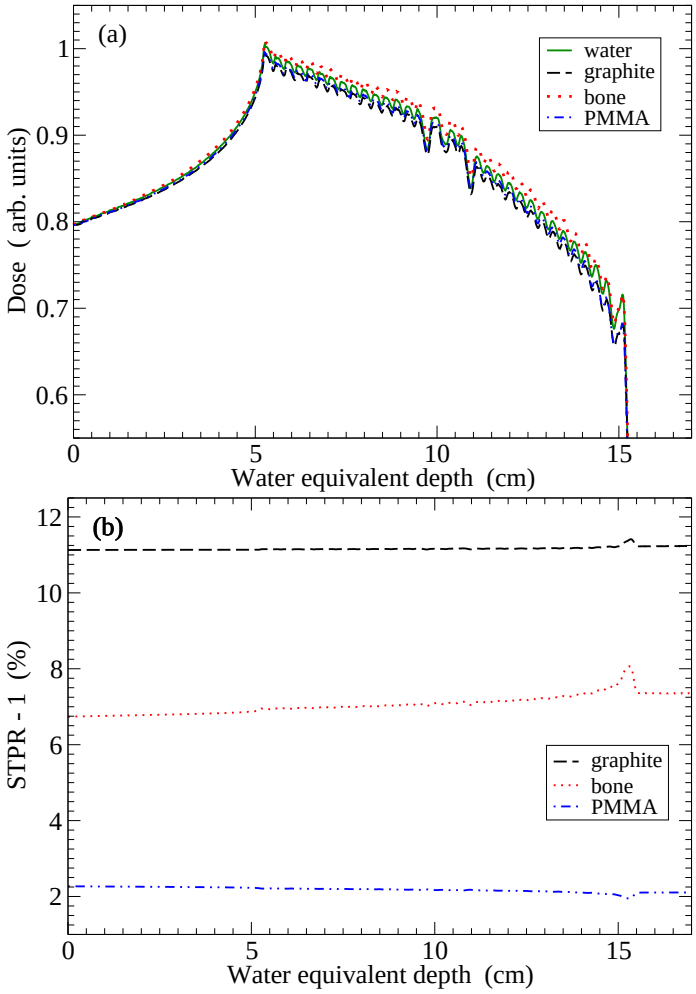

Figure 3. Like Fig. 2 but for a carbon ion spread-out Bragg-peak optimized for a flat *biological dose equivalent* distribution in water.

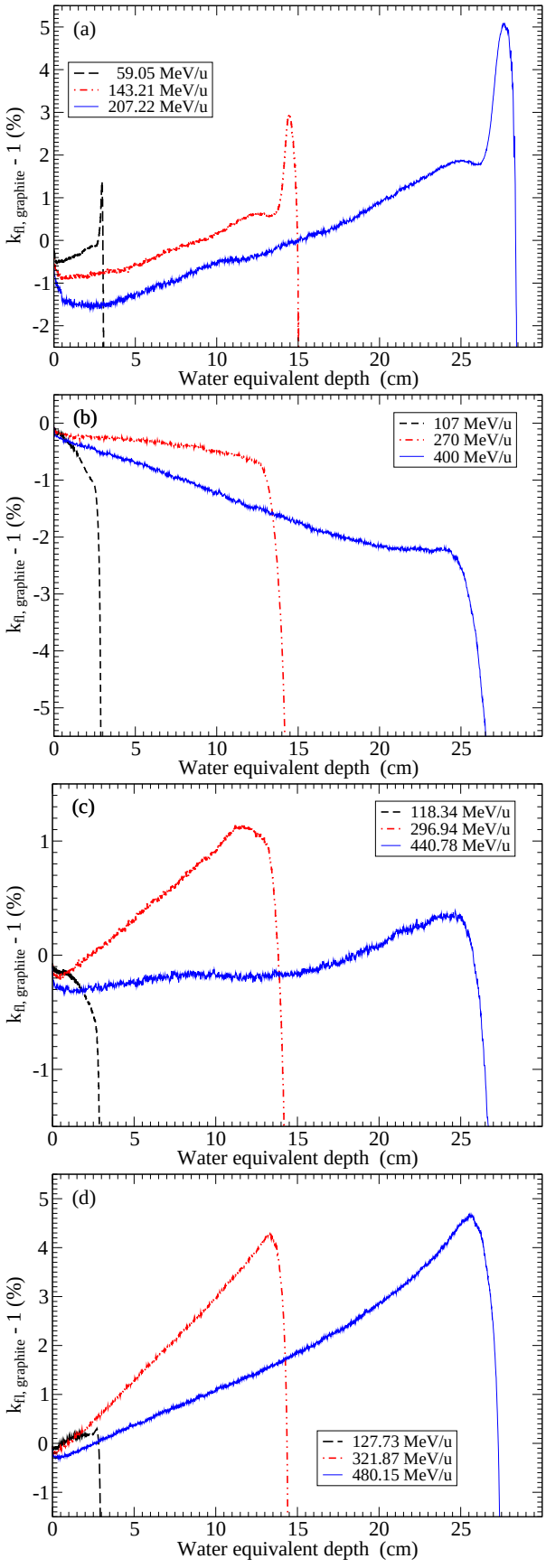

Figure 4. Fluence correction factor for graphite as a function of water equivalent depth obtained with Eq. (7) for different primary ions. (a) Protons, (b) carbon ions, (c) nitrogen

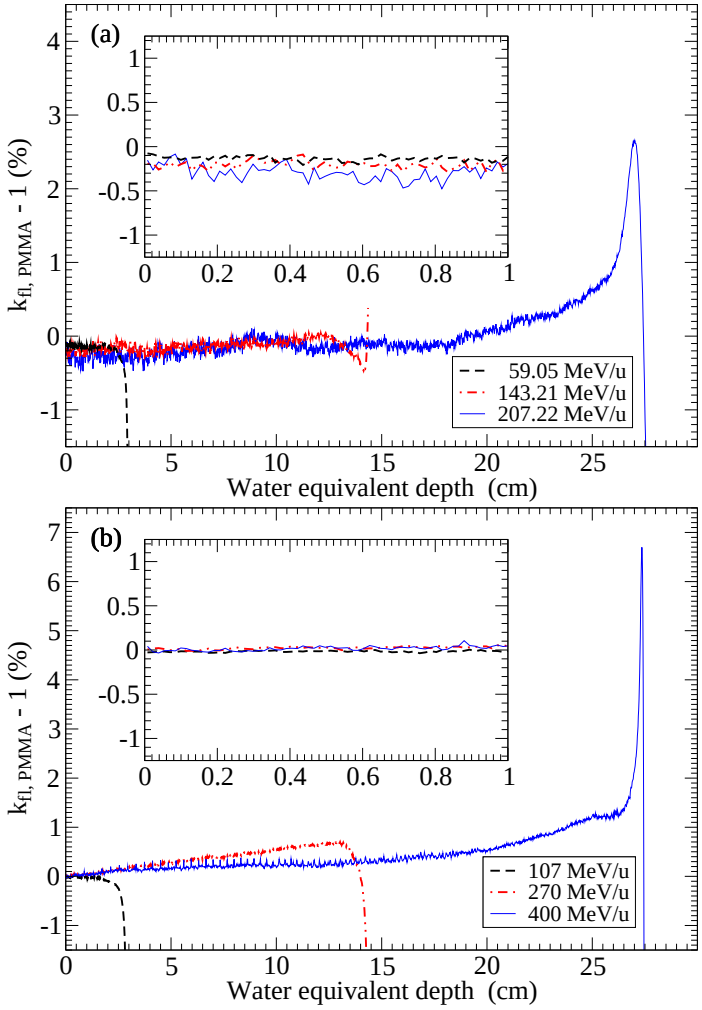

Figure 5. Like Fig. 4 but for PMMA. The inset shows the first cm on an enlarged scale. (a) Protons, (b) carbon ions.

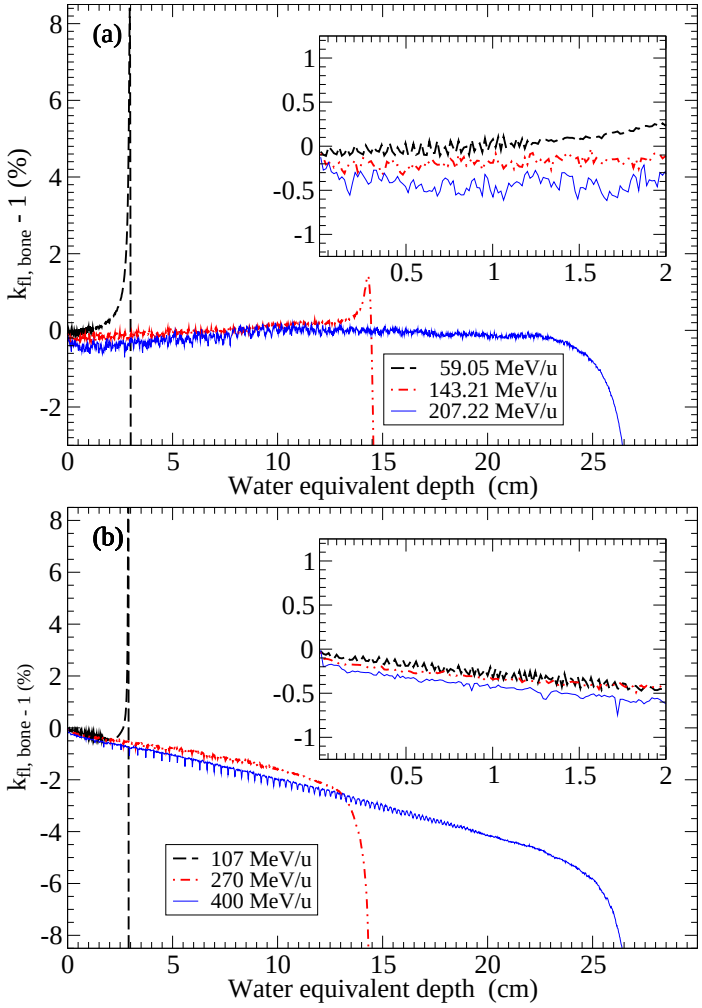

Figure 6. Like Fig. 4 but for bone. The inset shows the first two cm on an enlarged scale. (a) Protons, (b) carbon ions.

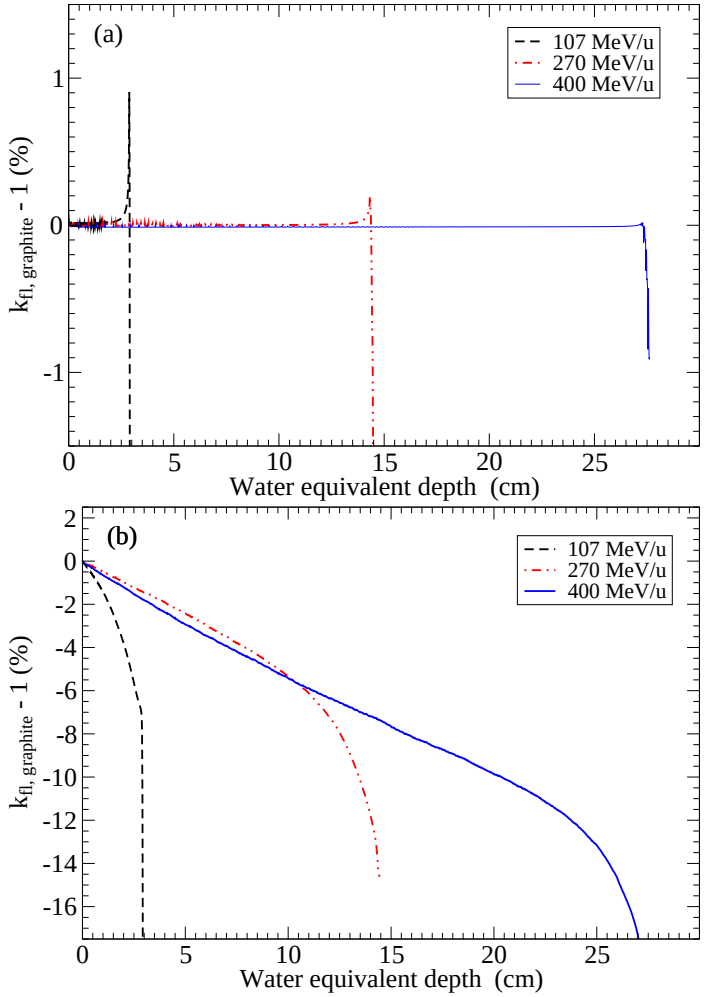

Figure 7. Fluence correction factor for graphite as a function of water equivalent depth for carbon ions obtained with Eq. (7). (a) Non-elastic nuclear interactions are not accounted for. (b) It is only accounting for the fluence of the primary ions, i.e. no sum over particle types i. See the text for explanation.